Marine Pollution Bulletin
July 2023, Volume 192 Pages 115059 (14p.)
https://doi.org/10.1016/j.marpolbul.2023.115059
https://archimer.ifremer.fr/doc/00838/94972/

Larval dispersal of pearl oysters *Pinctada margaritifera* in the Gambier Islands (French Polynesia) and exploring options for adult restocking using *in situ* data and numerical modelling

Bruyère Oriane [1, *], Chauveau Mathilde [1, 5], Le Gendre Romain [2], Liao Vetea [3], Andréfouët Serge [1, 4]

[1] IRD, UMR 9220 ENTROPIE (Institut de Recherche pour le Développement, Univ de la Réunion, IFREMER, Univ. Nouvelle-Calédonie, CNRS), BPA5, 98948 Noumea, New Caledonia
[2] Ifremer, UMR 9220 ENTROPIE (IRD, Univ. Réunion, IFREMER, Univ. Nouvelle-Calédonie, CNRS), BP 32078, 98897 Nouméa Cedex, New Caledonia
[3] Direction des Ressources Marines, BP 20, 98713 Papeete, French Polynesia
[4] IRD, UMR-9220 ENTROPIE (Institut de Recherche pour le Développement, Université de la Réunion, IFREMER, CNRS, Université de la Nouvelle-Calédonie), BP 49 Vairao, Tahiti, French Polynesia
[5] EPTB Gardons (Territorial Public Establishment of the Gardons rivers Basin), Nîmes, 30000, France

* Corresponding author : Oriane Bruyère, email address : oriane.bruyere@ird.fr

Abstract :

Black pearl farming is the second source of French Polynesia income after tourism, and Gambier Islands are the main farming sites. Gambier main lagoon contains several sub-lagoons critical for pearl oyster rearing and spat collecting (SC). The Rikitea lagoon, traditionally had good SC rates in the warm season which ensured steady supplies of oysters for black pearl production. However, since 2018, SC has abruptly decreased. To assess the factors affecting SC, Gambier lagoon hydrodynamics was investigated in 2019–2020 to calibrate a hydrodynamic model and simulate larval dispersal around the SC areas. The model shows the strong wind influence on larval dispersal and accumulation patterns and suggests that windy months in the warm season as it can occur during La Niña episodes can explain recent poor SC. Larval dispersal scenarios also informed on best locations to perform adult oyster restocking, a practice that can also enhance SC on the long term.

Highlights

► Gambier is the most important pearl farming site of French Polynesia. ► Hydrodynamic conditions in Gambier are studied during the spat collection season. ► A MARS3D hydrodynamical model is validated against *in situ* data. ► The model is used to simulate pearl oyster larval dispersal. ► The model identifies periods of low wind as critical for successful spat collection.

Keywords : MARS3D, Pinctada margaritifera, Connectivity, Aquaculture, Lagoon, Pearl farming

1. Introduction

In the past 30 years, pearl farming has considerably grown in French Polynesia with a quick expansion phase between 1995 and 2003, followed by more difficult times due to overproduction and poor market management (Andréfouët et al., 2012, 2022). Nowadays, it constitutes the second economic sector employing ~1300 workers on 28 atolls and islands. A single oyster specie is exploited by farmers, the black-lipped *Pinctada margaritifera*, a common bivalve species in the Indo-Pacific region but very abundant in several Tuamotu and Gambier lagoons of French Polynesia (Bionaz et al., 2022). Due to the natural abundance of this specie in a high number of lagoons, the French Polynesia black pearl industry soared based on larvae recruitment and spat collection onto artificial substrates. However, the juvenile collection efficiency is temporally and spatially variable with a decreasing success observed by farmers in the past years (Andréfouët et al., 2022).

To inform black pearl farming management, nearly 40 years of significant research efforts have investigated the environmental (physical and biological) factors controlling *in fine* spat collection, including physical meteorological forcing, trophic networks and biogeochemical processes (Lefebvre et al., 2012, 2022; Rodier et al., 2021), adult reproduction (Fournier et al., 2012), larval dispersal (Thomas et al., 2012a,b, 2014, 2016), and experimental collecting (Lo-Yat et al., 2022). Most recent integrated studies have attempted to combine these *in situ* data with numerical circulation models to better understand intra-lagoon larval dispersal through the computation of connectivity matrices according to different weather and trophic conditions (Thomas et al., 2016; Andréfouët et al., 2021). Connectivity matrices are then used to make suggestions for adult oysters restocking locations (André et al., 2022a, Violette et al., 2023), since there are evidences that decreasing natural oyster stocks can ultimately affect spat collection (Reisser et al., 2020).

Despite this amount of research, there is still much to do to inform management of pearl farming atolls. In particular, only three French Polynesia atolls (namely Ahe, Takaroa and Raroia, which represented semi-closed to semi-open lagoons) thus far benefit from 3D circulation models (Dumas et al., 2012; Violette et al., 2023; Le Gendre et al., in prep.). But there are many more critical sites for pearl farming in the Tuamotu atolls, such as Apataki, Katiu, Arutua or Takapoto. In addition, the Gambier Archipelago, which is not an atoll but a

large open lagoon surrounding high islands in the far southeast of French Polynesia. This site represents the first French Polynesia pearl farming lagoon as in 2021 (latest available statistics). Pearl culture is an important economic resource for local population of Gambier islands (André et al., 2022b). It represents approximately 25% of the total area of pearl farming concessions in French Polynesia, and 33% of the country pearl production which amounts to 40M€. Geomorphologically speaking, it is also the most complex coral reef site of French Polynesia (Andréfouët et al., 2008) due to its partly drowned barrier reef, numerous bays and patch reefs, deep and shallow passages, and enclosed lagoons. However, due to its remoteness, Gambier remains poorly studied thus far, with limited biological knowledge usable for pearl farming management (Le Moullac et al., 2012; Liao 2019; Lo-Yat et al., 2022). In 2019, a program was launched to study the physical circulation of the lagoon, and implement a numerical 3D hydrodynamic model for this complex site. The study also included a new natural oyster stock assessment which is reported in Bionaz et al. (2022).

To the best of our knowledge, this study at the scale of an island is one of the very few offering in a single integrated package: new *in situ* physical oceanography observations, 3D numerical modelling, connectivity (larval dispersal) modelling, and application for a concrete management problem. One example of such integrated studies addressed coral larvae dispersal between Hawaiian Islands for the identification of marine protected areas (Storlazzi et al., 2017). Specifically, we report on the *in situ* physical measurements performed on the Gambier forereefs and lagoons, the development of a high spatial resolution 3D numerical circulation model and its validation using the *in situ* data, and its preliminary use to suggest oyster restocking sites with the goal of ultimately facilitating spat collection. This is motivated by the last spat collection rates in Gambier, which have been extremely low the past four years (2020-2023, Liao pers. obs.). Farmers and managers, are very concerned for the sustainability of their activities (André et al., 2022b) and this study sheds new lights critical to understand and manage pearl oyster spat collection.

2. Material and methods

2.1 Study site

The Gambier Islands are located in the Southeast region of French Polynesia (23°07′ S – 134° 58′ W) (Figure 1). The lagoon has a diamond-shaped form and surrounds seven high islands: Mangareva which is the main inhabited island, Aukena, Taravai, Akamaru, Kamaka and Agakauitai (Figure 2).

The Gambier lagoon has a complex geomorphology. The west and south sides are opened to the ocean with a submerged reef contrary to the east and north sides where the lagoon is closed by an intertidal and emerged reef barrier. In some sections, the reef rim is cut by several shallow passages named *hoa* (depth ~50 cm) allowing water exchanges between lagoon and ocean. Two deep passes, west and south are also prominent features and are used by large ships to access the capital Rikitea on Mangareva Island. The average depth of the domain is 24.5m with a maximum reaching 71 m on the southeastern coast of Mangareva Island. The bathymetry is complex and form several basins, including the Rikitea enclosed lagoon bordered by Mangareva and Aukena islands that is historically the prime spat collection site.

Since 2017, a designated spat collection area has been implemented, empirically selected due to its good historical collecting rates. Therefore, all spat collectors need now to be deployed in this area which includes the Rikitea enclosed lagoon, and part of the deep channel south of Aukena island (Figure 2). Spat collection remains critical in Gambier and there are no alternative sources that can provide the millions of oysters raised every year by the pearl farms. While pilot nurseries have been established, thus far they only aim to produce a limited number of oysters with specific color mantle that are inserted with a nucleus in the receiving oysters during the grafting phase.

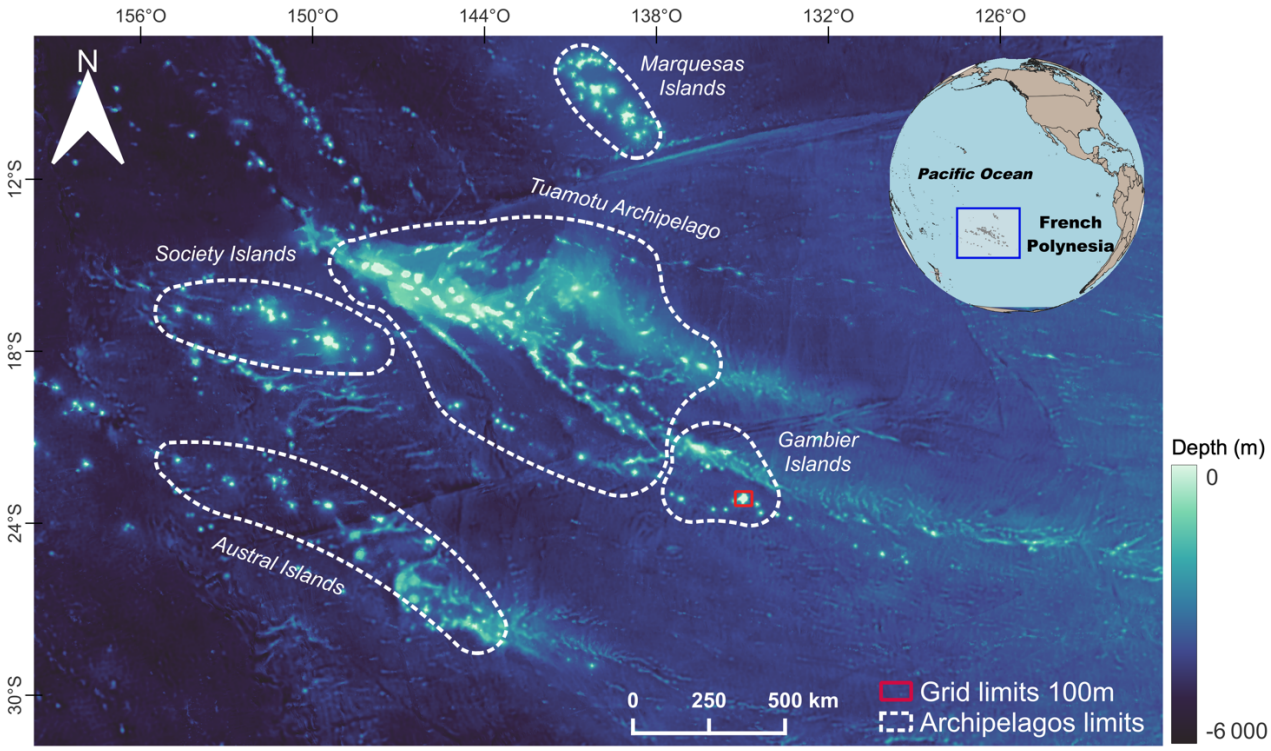

Figure 1: Gebco bathymetry map of French Polynesia Islands and archipelagoes. The red box shows the Gambier grid model dimension.

2.2 Hydrodynamic measurements

A variety of physical oceanographic instruments have been deployed from mid-June to late October 2019 (Leg1) and from late October 2019 to late February 2020 (Leg2) (Table 1). Autonomous data loggers including inclinometer drag-tilt current meters (Marotte HS), and compact temperature and pressure loggers such as RBRduet T.D and temperature loggers SBE56 were deployed in Leg1. The second leg includes six acoustic doppler current profilers (ADCP) moored to complement the instruments listed above and deployed since Leg 1. The second leg covers the period that is usually the beginning of the spat collection season, as farmers start deploying their collectors when lagoon temperature start to rise, which can be interpreted as a trigger for oyster spawning (Sangare et al. 2020), although Le Moullac et al. (2012) did not relate the first spawn of their monitoring period, in December 2002 to temperature.

The sampling strategy was to focus on the lagoon circulation at key locations and specifically for the entrances of the Rikitea enclosed lagoon so critical for spat collection. The lagoon circulation has been studied at Leg 2 with four ADCP Sentinel (V20 – V50) deployed in deep

channels and lagoon locations (Fig. 2, Table 1) and two Nortek Aquadopp in shallower regions. In particular, the two Aquadopp and one V50 were positioned to characterize the flux of water at the border of the Rikitea lagoon. Near-bottom currents in shallower reef flats were measured with Marotte HS on three stations (Fig. 2), with two Marotte duplicating the Aquadopp sensors. This was done to compare the low-cost inclinometers Marotte HS with the ADCP Aquadopp data. Pressure sensors deployed on each side of Gambier informed on the oceanic wave conditions. To characterize incident waves, five RBRduet T.D measuring temperature and pressure at 1Hz have been moored on the external reef slope on approximately 10m depth (Fig. 2, Table 1). Four other RBRduet T.D loggers were fixed inside the lagoon to record tide and surge signals. Pressure data have been processed using the Fourier transform to apply the linear wave theory (method used in Aucan et al., 2017) to acquire a water elevation time series at every minute and waves parameters (Significant wave height, wave period, etc.) at hourly frequency. Surges data have been performed by applying Demerliac tide filter (Demerliac, 1974) on elevation data to remove the tide signal with a 72h window. Finally, temperature data were recorded at high sampling frequency by most sensors (RBRduet, SBE56, Sentinels, Marotte HS). On four stations (L01-L04), SBE56 sensors were vertically deployed at 3m and 20m depth, combined with a RBR at 7-8m to observe the water column stratification.

Beyond the provision of key physical data on temperature, wave parameters, water levels and currents, this data set allowed to perform the calibration and the validation of the Gambier 3D hydrodynamic model to improve its realism (see below).

2.3 Wind data

A Météo France (MF) weather station measured wind speeds and directions at 91 altitude meters for a location in the southeast of Mangareva Island (Figure 2), nearby the Rikitea lagoon. MF data could be better suited to specifically study the Rikitea lagoon, but for the general situation over the entire Gambier lagoon, due to local orographic effects and as recommended by Laurent and Maamaatuaiahutapu (2019), we preferred to use the synoptic ERA5 data, a strategy already applied for other pearl farming sites (Thomas et al., 2012; Andréfouët et al., 2021). Wind data since 2002 were retrieved from the ERA5 reanalysis model

at 0.25° spatial resolution at an hourly time step, providing U and V components at 10m altitude. Data were extracted at one location, positioned inside Gambier lagoon (134.96401 W; 23.13010 S).

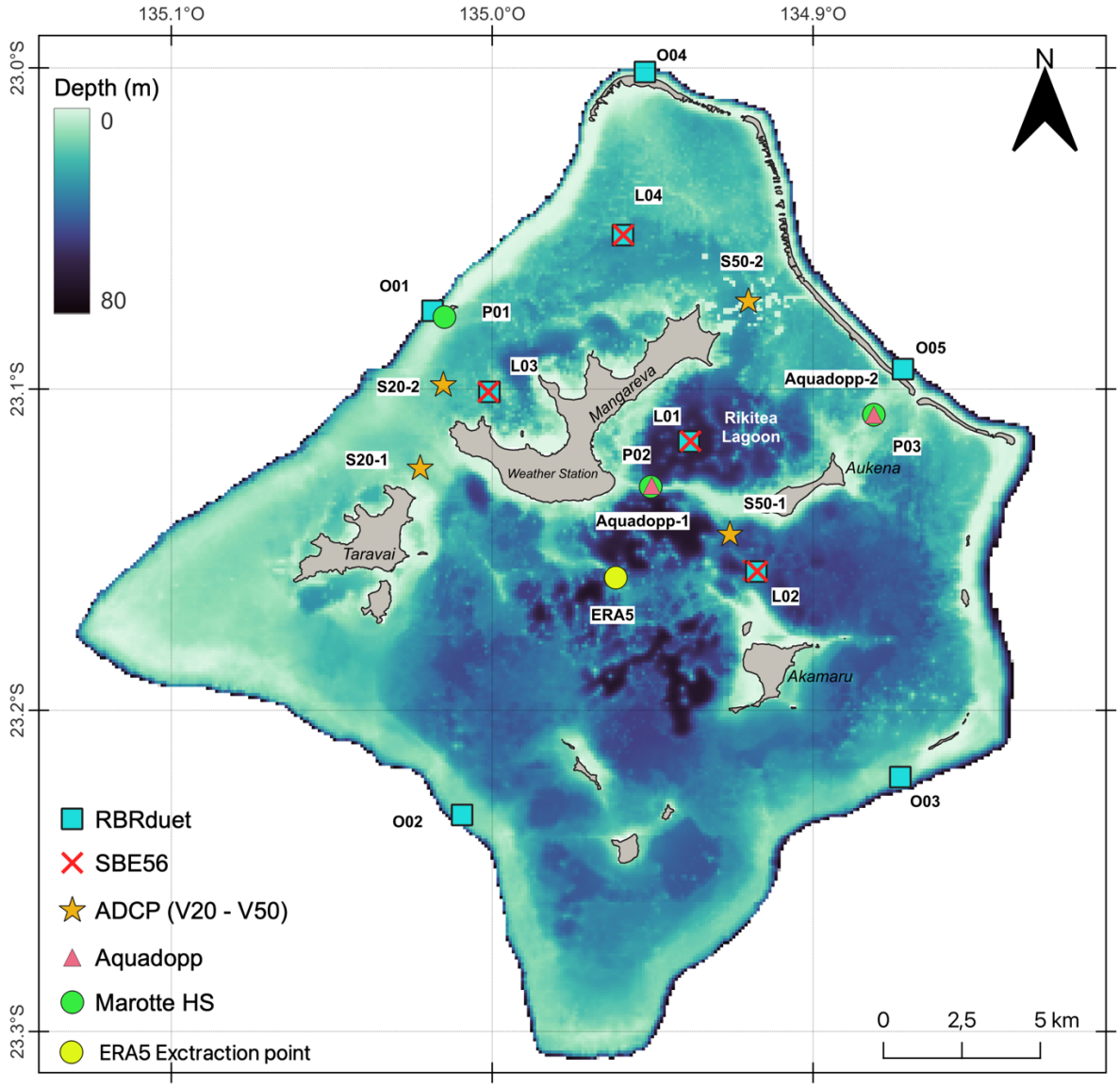

Figure 2: Gambier lagoon bathymetry and locations of in situ sensors deployed between June 2019 and February 2020. The two current meter Aquadopp were doubled with inclinometers Marotte sensors. In L01 to L04, sensors were positioned vertically, with two SBE56 temperature sensors moored at ~20 and 3m depth along with an RBRduet T.D pressure sensor in intermediate position at ~7-8m depth. See Table 1 for deployment details for each sensor. Rikitea lagoon is shown as the prime spat collecting site in Gambier. ADCP: Acoustic Doppler Current Profiler.

Table 1: Description of deployed loggers in Gambier lagoon between June to November 2019 (Leg 1) and November 2019 to February 2020 (Leg 2).

Station	Longitude (W)	Latitude (S)	Instrument	Raw parameters	Freq	Depth	Processed parameters	Legs
P01	135.01491	23.07758	Marotte HS	Current – temperature	1 min	5m	Temperature – current speed & direction	1,2
P02	134.95062	23.13042	Marotte HS	Current – temperature	1 min	2m	Temperature – current speed & direction	1,2
P03	134.88107	23.10799	Marotte HS	Current – temperature	1 min	3m	Temperature – current speed & direction	1,2
O01	135.01859	23.07563	RBRduet T.D	Temperature – pressure	1 Hz	12m	Temperature – wave height & period – water level	1,2
O02	135.00941	23.23259	RBRduet T.D	Temperature – pressure	1 Hz	13m	Temperature – wave height & period – water level	1,2
O03	134.87282	23.2208	RBRduet T.D	Temperature – pressure	1 Hz	13m	Temperature – wave height & period – water level	1,2
O04	134.95241	23.0013	RBRduet T.D	Temperature – pressure	1 Hz	11m	Temperature – wave height & period – water level	1,2
O05	134.87201	23.09379	RBRduet T.D	Temperature – pressure	1 Hz	9m	Temperature – wave height & period – water level	1,2
L01	134.93892	23.1164	SBE56	Temperature	10 s	3m	Temperature	1,2
			SBE56	Temperature	10 s	20m	Temperature	1,2
			RBRduet T.D	Temperature – pressure	1 Hz	7m	Temperature – wave height & period – water level	1,2
L02	134.918639	23.15641	SBE56	Temperature	10 s	3.5m	Temperature	1,2
			SBE56	Temperature	10 s	20m	Temperature	1,2
			RBRduet T.D	Temperature – pressure	1 Hz	7m	Temperature – wave height & period – water level	1,2
L03	135.00069	23.10083	SBE56	Temperature	10 s	3m	Temperature	1,2
			SBE56	Temperature	10 s	20m	Temperature	1,2
			RBRduet T.D	Temperature – pressure	1 Hz	8m	Temperature – wave height & period – water level	1,2
L04	134.95937	23.052039	SBE56	Temperature	10 s	3m	Temperature	1,2
			SBE56	Temperature	10 s	20m	Temperature	1,2
			RBRduet T.D	Temperature – pressure	1 Hz	8m	Temperature – wave height & period – water level	1,2
S50-01	134.92593	23.14531	ADCP Sentinel-V50	Current – temperature – pressure	20 min	35m	Temperature – current speed & direction – water level	2
S50-02	134.92017	23.07273	ADCP Sentinel-V50	Current – temperature – pressure	20 min	31m	Temperature – current speed & direction – water level	2
S20-01	135.02245	23.12469	ADCP Sentinel-V20	Current – temperature – pressure	10 min	17m	Temperature – current speed & direction – water level	2
S20-02	135.01524	23.09875	ADCP Sentinel-V20	Current – temperature – pressure	10 min	19m	Temperature – current speed & direction – water level	2
Aquadopp-1	134.95030	23.13006	Nortek Aquadopp	Current – temperature – pressure	10 min	9m	Temperature – current speed & direction – water level	2
Aquadopp-2	134.88107	23.1080	Nortek Aquadopp	Current – temperature – pressure	10 min	3m	Temperature – current speed & direction – water level	2

2.4 Hydrodynamic model

In this study, the numerical 3D hydrodynamic model MARS3D (Model for Application at Regional Scale) has been used to model Gambier Islands. A detailed description of the model foundation and hydrodynamics equation is provided by Lazure and Dumas (2008). For this study, a single grid encompasses entirely the Gambier lagoon with a spatial resolution of 100 m and 30 sigma layers on vertical axis from the bottom to the surface boundary layers. At the

open boundaries, the model is forced by astronomical tides using a harmonic recomposition of FES2012 (Finite Element Solution) solution containing 32 tidal constituents at 1/16° resolution. The model is forced at the open boundaries using the global oceanic reanalysis product GLORYS12V1 (currents, levels, temperature and salinity) at daily time step. Meteorological conditions at hourly time step were extracted from the MF weather station (Figure 2). For all simulations a spin-up time of 20 days was applied to reach a state of statistical equilibrium. The model is always initialized with the aforementioned forcings (tide, regional currents and weather conditions).

In situ observations were compared to assess the realism of the modeled current speeds and directions in specific wind conditions, by using measures of statistical fit for the entire time series, namely the coefficient of determination R^2 of the linear regression and the root mean square error (RMSE), which indicates the average difference between modeled and *in situ* values. The validation of the model is based on the agreement between *in situ* and modeled values and if the agreement is satisfactory, the model is deemed suitable to simulate larval dispersal during at least the same wind conditions that occurred during field work.

The model is also using a newly created bathymetric grid. To achieve an accurate high-resolution grid for MARS3D model (100 m spatial resolution), different sources of bathymetry data have been merged. Acoustic surveys were available for the Gambier lagoon through the French Hydrographic and Oceanographic Service (SHOM) depth soundings acquired across several decades. A recent multi-beam echo sounder survey also provided extended coverage (~100 km^2 of the lagoon) at very high resolution. However, soundings in shallowest areas and intertidal zones around islands and the northern lagoon were missing. To fill this gap, bathymetry data have been generated using a Sentinel-2 optical satellite image and following the method presented in Amrari et al. (2021) for shallow (< 15m depth) and clear water lagoons. For this, we took advantage of the extensive *in situ* bathymetry data sets for calibration and validation. Oceanic bathymetry was obtained using the global terrain model GEBCO. To fill gaps, all these point data were interpolated using a kriging and smoothing method as implemented in the MARS3D package.

2.5 Larval dispersal modelling

Once validated, the numerical model was used to simulate the trajectories of larvae and assess what would be their fate after a pelagic larval duration (PLD) within its most likely range around 20 days (15 to 25 days) (Thomas et al., 2014; Sangare et al., 2020). In an oyster restocking context, we aim to identify spawning locations that will potentially maximize spat collection, in other words, the spawning locations from which larvae will accumulate the most at the end of their PLD in the designated spat collecting areas. In practice, once these locations have been identified, they will be used by farmers and the governmental pearl farming management entity (the *Direction des Ressources Marines*, or DRM) for restocking.

The biophysical model combining Lagrangian advection/dispersal module computed thanks to a non-naïve random walk (Visser. 1997) and vertical swimming of bivalve larvae according to the day/night cycles has been implemented into MARS3D code (Thomas et al., 2012a; Thomas et al., 2012b; Andréfouët et al., 2021).

To identify potential restocking and spawning sites, eighteen potential restocking/spawning stations (S01 to S18) were quasi-systematically positioned between Mangareva and Aukena islands (Figure 3). These stations were selected to not overlap areas where the oyster stock is significant (see Bionaz et al., 2022), under the rationale that restocking is needed first in depleted areas. One station (S17) was positioned in the north lagoon for reference, and one on the west side of Mangareva near dense pearl farms (Taku Bay, S18). S15 is a station located just south of the Mangerava-Aukena sill, where most of the oyster stock is present (Bionaz et al., 2022). Each spawning station was simulated by a virtual circular patch of 400m diameter, from which larvae can be released randomly between 0 and 15 m depth.

Four scenarios were studied.

- A “no-wind” scenario 1, hence with circulation only driven by tide. It is considered as a neutral, reference, scenario. The dispersal duration was set at 26 days.
- A “NE wind” scenario 2, with a stationary wind blowing during the entire dispersal period. This scenario is justified by the dominance of the NE wind during the 2019-2021 January summer months, with an average speed and direction of 5.7 $m.s^{-1}$ and 60° respectively (from ERA5 data). The dispersal duration was set at 26 days.

- A first realistic scenario 3, for which the wind observed daily between 29/01/2020 and 13/02/2020 is applied. Realistic scenarios consider actual wind variations, including sharp shifts in direction and speed. The effects of these transitions on dispersal can thus be assessed.
- A second longer realistic scenario 4, for which the wind observed between 22/01/2020 to 11/02/2020 is used to force the circulation. It overlaps the period of the third scenario (29/01/2020 and 13/02/2020), but present different wind conditions in the initial week.

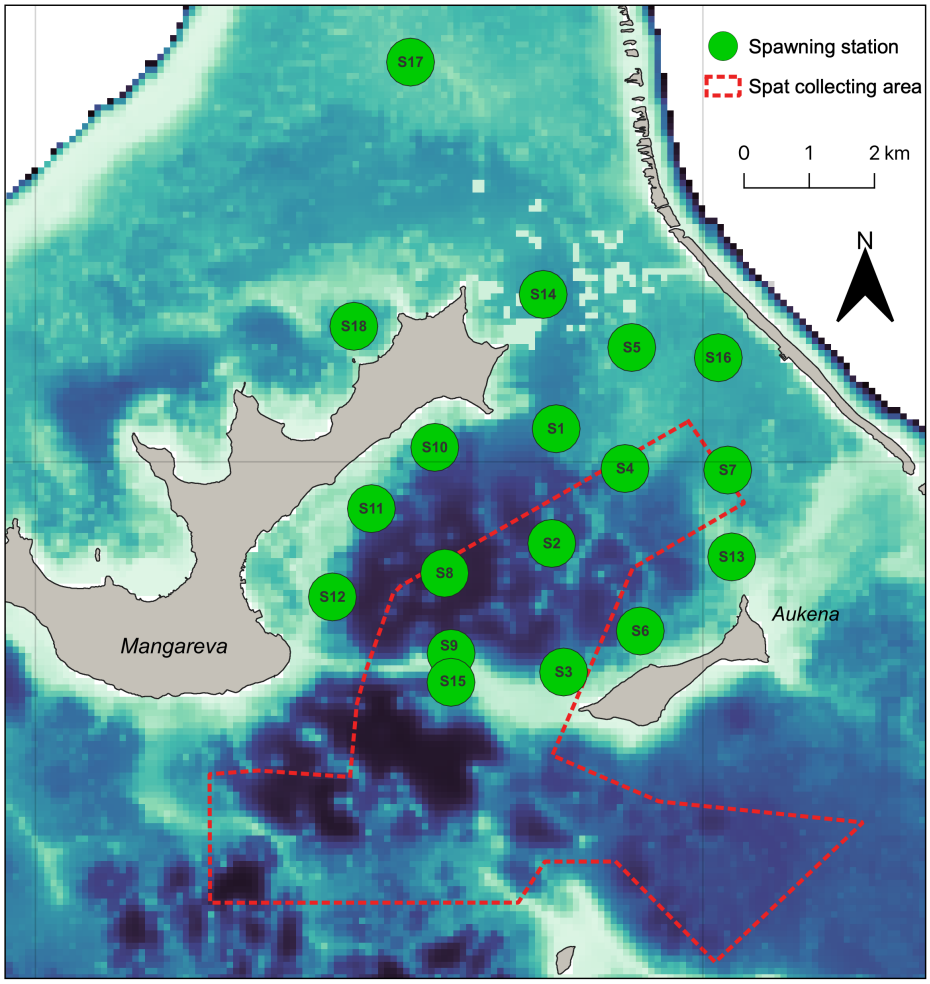

Figure 3: Locations of potential restocking sites (green circles) selected for the Rikitea lagoon, and outside of it. The red dotted contour is the spat collection designated area.

In total we released approximately 150 000 larvae due to model simulation time limitation. This number corresponds to previous Lagrangian modelling exercises (for instance Thomas et al., 2016 released 166 692 particles in Ahe atoll). The number of larvae could be different for each station (between 6573 and 8650 larvae), as we set manually a number of larvae per

depth level (equal to 1m) in order to get a similar number of larvae per stations. Then depending on stations and their depth, the number of larvae per level ranged from 550 to 700. Trajectories are saved for each larva every 6h. After the simulation, post processing is required to census every day the percentage of larvae within the designated spat collection areas, or outside. These percentages allow visualizing the dispersal dynamics, in particular how fast would larvae leave, or enter, the spat collection area, or if cloud of larvae can leave and re-enter multiple times the area. Larvae reaching the coastline remain in the water domain and can bounce back into the lagoon. They are not considered dead. However, larvae ending outside the domain are considered dead during the post-processing phase. There are no *in situ* larval census data available in Gambier to confront simulations with *in situ* observations of larval densities, a common gap in dispersal studies. In a pearl farming context, only Thomas et al. (2012a) in Ahe Atoll have managed to document the dispersal of spawns thanks to a considerable field sampling effort of four one-month leg of daily sampling. This effort has never been reproduced.

3. Results

3.1 General oceanographic and atmospheric conditions during the observation legs

Figure 4 provides for Legs 1 and 2, the hourly ERA5 wind data (speed and direction) and wave data from RBRduet T.D sensors moored outside the reef on oceanic slopes. Figure 5 provides for Legs 1 and 2 the temperature data from one lagoon and one oceanic station, as well as tide and surge time series for the oceanic station O03. Considering the consistency of temperature, tide and surge data between locations, not all stations are shown.

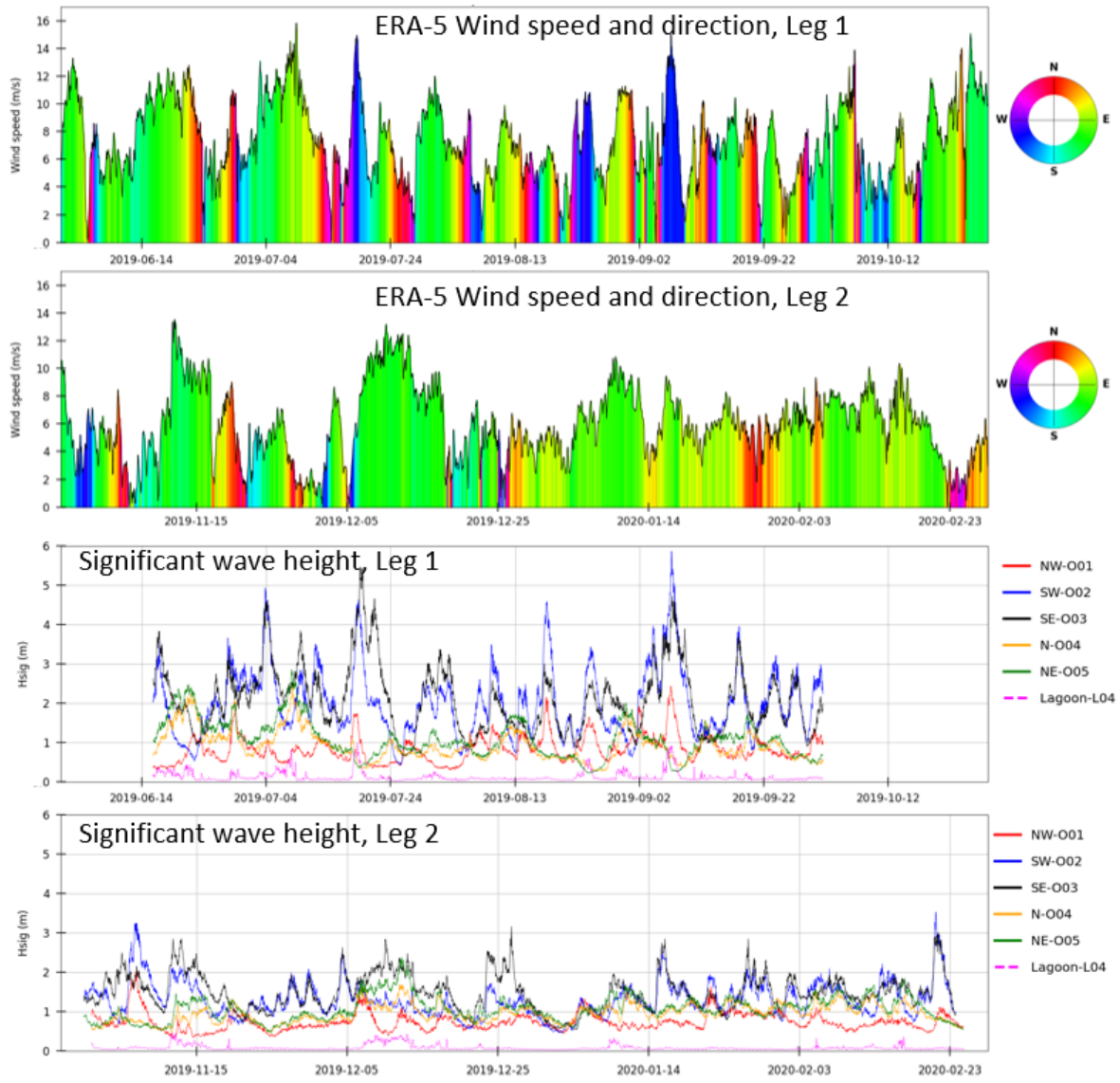

Figure 4: Wind conditions (speeds and directions) during Leg 1 and Leg 2, and significant wave heights measured by the RBRduet T.D sensors moored on the oceanic forereefs (stations O01-O05, labelled here with their orientations) and for one lagoon station (L04). Note that the y-axis scales are the same for both legs. By convention, wind direction is the angle from which the wind is coming from (0°=North).

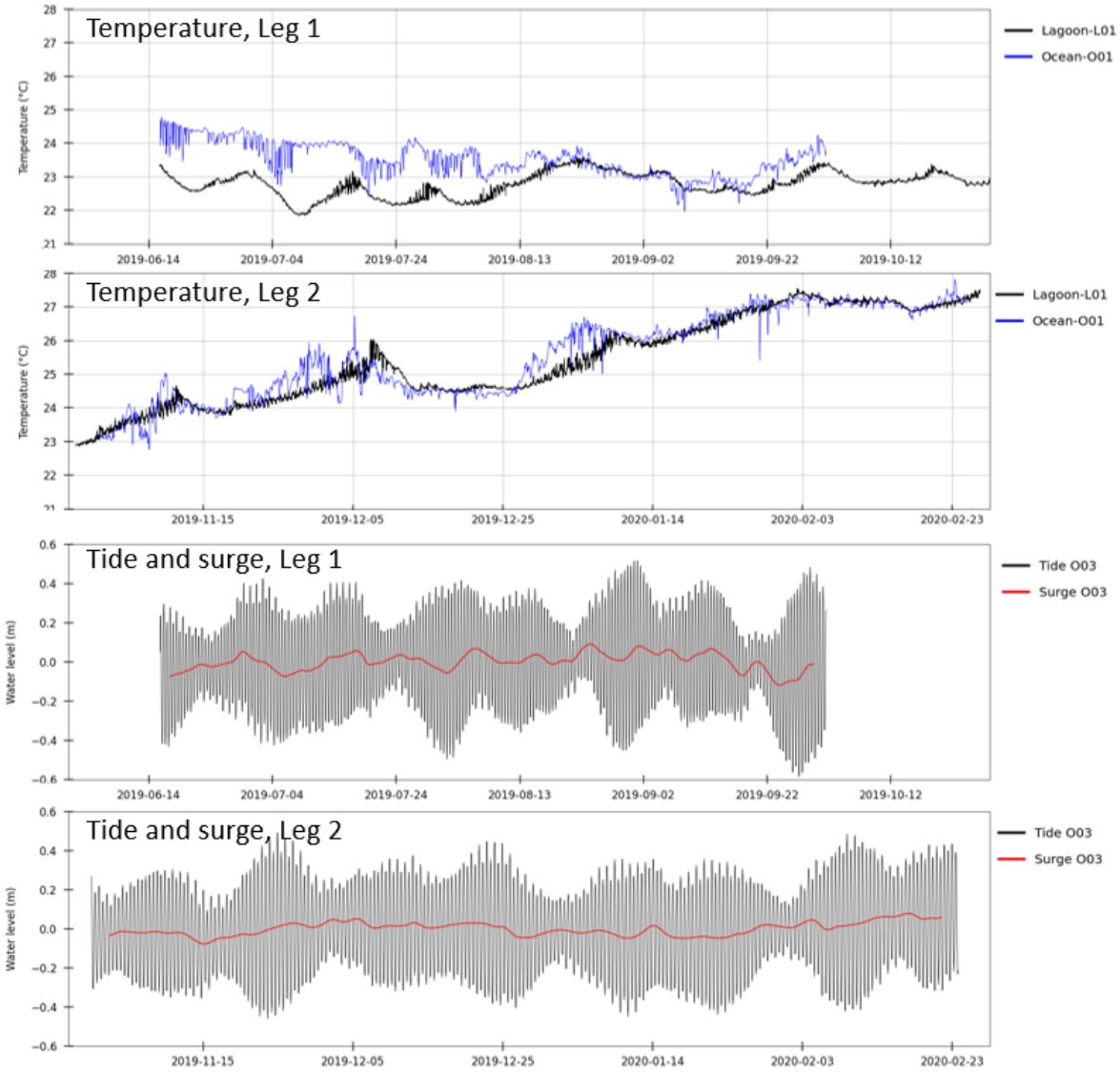

Figure 5: For Leg 1 and Leg 2, temperature is observed from one oceanic (O01) and one lagoon stations (L01). Only one sensor in each geomorphological strata considering their consistency. Tide and surge on the ocean are shown for the oceanic station O03. Note that the y-axis scales are the same for both legs.

Figures 4 and 5 show that the Leg1 and Leg2 experienced contrasted wind and wave conditions. Overall, the Leg 1 included much more variable and stronger wind and higher waves than Leg 1. The south-exposed pressure sensors recorded only two short occurrences of a 3m significant wave height (Hsig) in Leg 2, while these were common conditions in Leg 1, peaking at 6 meter around 9-10 September. The two most energetic south swell events in Leg 1 also corresponded to episodes of strong southwest wind. Leg 2 is dominated by southeast

to northeast wind, with short episodes of north, west and southwest winds. Leg 2 also had four periods of calm conditions, with low-speed wind (~2 to 3 $m.s^{-1}$) for few days (Figure 4).

Figure 5 shows only the temperature for one oceanic RBRduet T.D sensor and one lagoon sub-surface sensor as temperature ranges and trends were consistent between sensors in similar geomorphological zones, although deeper lagoonal SBE56 recorded a lower temperature than lagoon sub-surface temperature (not shown, but about 1°C difference). All lagoon sensors show stable conditions throughout the first Leg at ~23°C, then temperature increases starting early October 2019. The warming is steady during Leg 2 till end of February 2020 (>28°C) but three episodes of strong southeast winds (~10 m.s-1) cooled the lagoon (Figure 5). The oceanic sensor in Leg 2 follows the same trend as the lagoon sensor but ocean was warmer than the lagoon and still cooling during the first part of the Leg 1

Tide and surge data do not show a spectacular increase in water levels in Leg 1 during the periods of very high swells, confirming the very open nature of the Gambier lagoon (Figure 5).

3.2 Analysis of residual currents at Rikitea lagoon borders

To characterize the hydrodynamics of the Rikitea lagoon during Leg2, we focused on the daily residual currents (i.e., tidally corrected currents using Demerliac filter) measured at the locations of Aquadopp-1 & 2 and ADCP S50-2. Currents speed was projected depending on the main current direction axe (Figure 6) to better assess the relationships between currents and wind. The direction applied for the projections are respectively for AQ1 and AQ2, 359° and 292°, and 162° for S50-2. By convention, signs are set so that current flowing towards the Rikitea lagoon are positive. This analysis provides an overall tide-corrected balance of the inflows and outflows around the three main borders of the Rikitea lagoon. Residual currents are inspected versus the variations of wave and wind data that occurred during Leg 2. The time-series allows visualizing the influence of changing wind characteristics on the dynamic of the projected residual currents observed on the three instruments (Figure 6).

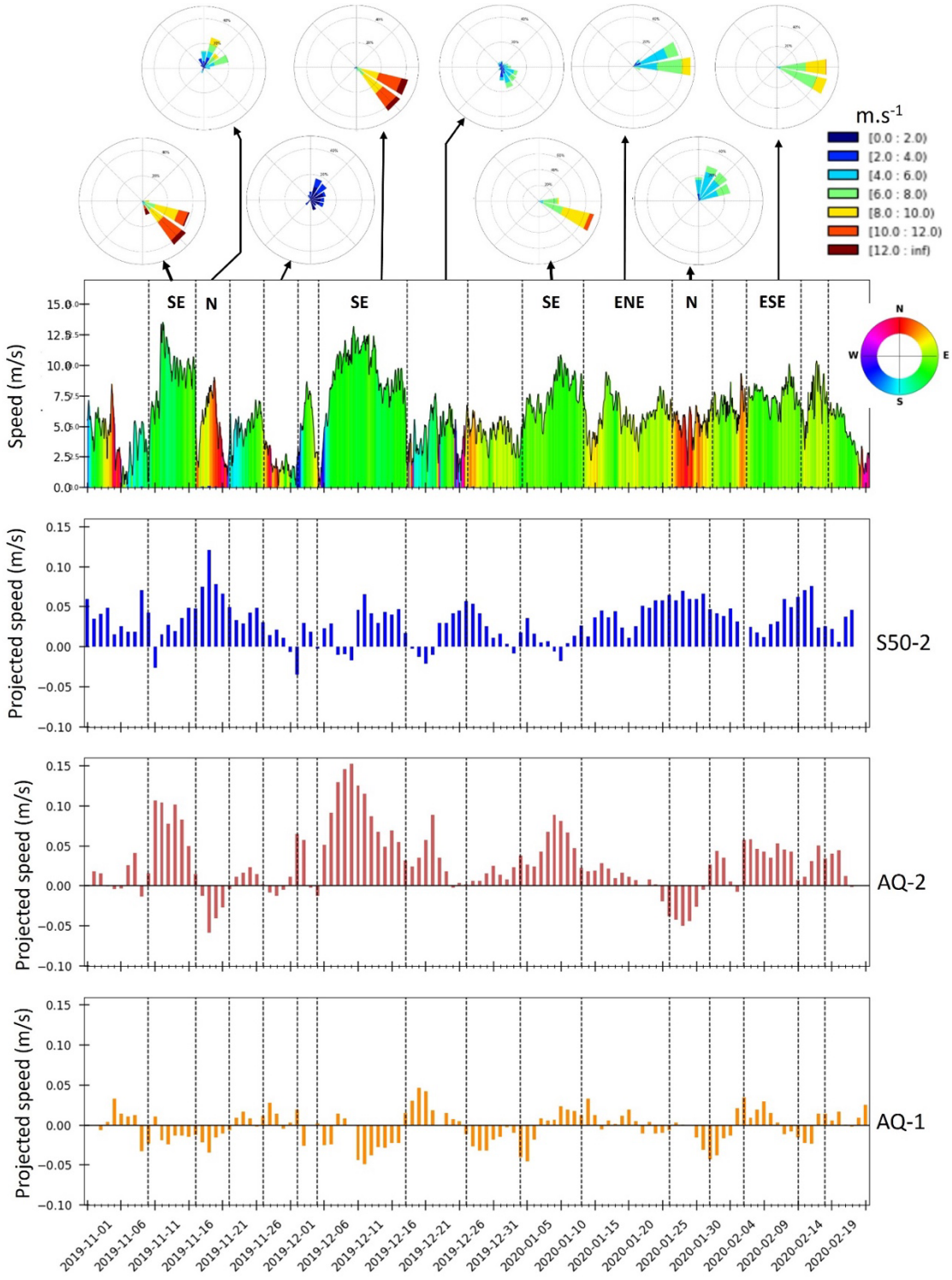

Figure 6: Effects of the wind on the residual currents for the three strategic locations bordering the Rikitea sub-lagoon in station S50-2, AQ-2 and AQ-1. The wind conditions are shown on top. The vertical bars show the limits between different wind directions and speed. The projected residual currents along their main directions highlight several specific responses at the level of each sensor for different winds. For instance, currents in AQ-2 have a dominant northwest direction (positive values on the projection) for winds coming from the southeast (green color). By convention, wind direction is the angle from which the wind is coming from (0°=North).

Figure 6 highlights first the dominant directions of residual currents for AQ-2 moored in the eastern side and for S50-2 situated in the northern part of the Rikitea lagoon. Residual currents are going mostly towards the Rikitea lagoon for these two sensors. Conversely, the residual currents observed at AQ-1 (south region of the lagoon) are more variable, and with less strength.

The behaviors of residual currents for the three sensors are strongly related to wind directions and strengths, then as a secondary factor to waves. However, it is necessary to keep in mind that the wave regime was low during the Leg 2 (Figure 4) and this may be different in the wave conditions of the first Leg. For Aquadopp-2 located on the sand flats east of Aukena Island, faster inbound residual currents occur when the winds are from southeast (peak 15th November 2019, 8th December 2019, and 7th January 2020). Northeast to southeast wind directions generate moderate inbound currents. Two short episodes of current leaving the lagoon (around 18th November 2019 and 27th January 2020) are characterized by north winds. Figure 6 also illustrates the dominant behavior of residual currents at the station S50-2, where the tide-corrected currents are virtually always going towards the Rikitea lagoon, although at lower speed when the wind blows from the southeast. Conversely, the Aquadopp-1 in the south of Rikitea lagoon is much more variable, with residual currents alternatively inbound or outbound, although east-southeast winds generally generate outbound current, likely to evacuate excess waters coming from the more exposed eastern reef flats, represented by Aquadopp-2.

The Leg 2 was instrumented at a period considered generally favorable for spat collection in the Rikitea lagoon. The results presented here confirm that the residual currents, hence offering a view of the balance of the exchanges once the tide is omitted, are rather indicative of larvae being able to remain in the Rikitea lagoon, thus explaining why this lagoon has been a major spat collecting site for the last three decades in the warm season. The Leg 1, in the cooler season does not have the same type of low energy forcing that characterizes the Leg 2, hence it is likely that residual currents during the first Leg may show a different perspective than in Leg 2. The complete dynamic, with tide included, need to be considered to really understand where and how larvae will travel, as tide-driven transport can also be significant. This is studied hereafter through the use of a 3D model.

3.3 Hydrodynamic model validation

The hydrodynamic model skills were assessed by comparing tide and depth-averaged current speeds from MARS3D model results *versus* the *in situ* data set covering the Leg 2 period. To visualize the data at full resolution, only the first two weeks of the Leg 2 are shown in Figure 7 and 8. Comparison between *in situ* data and modeled tide data is shown in Figure 7 for oceanic and lagoon RBRduet T.D sensors. The agreement is satisfactory: the model represents well tide cycles, as the R^2 and RMSE for oceanic station (O01) are 0.975 and 0.04m respectively. For lagoonal station (L04) the statistics are similar with R^2=0.96 and RMSE= 0.04m.

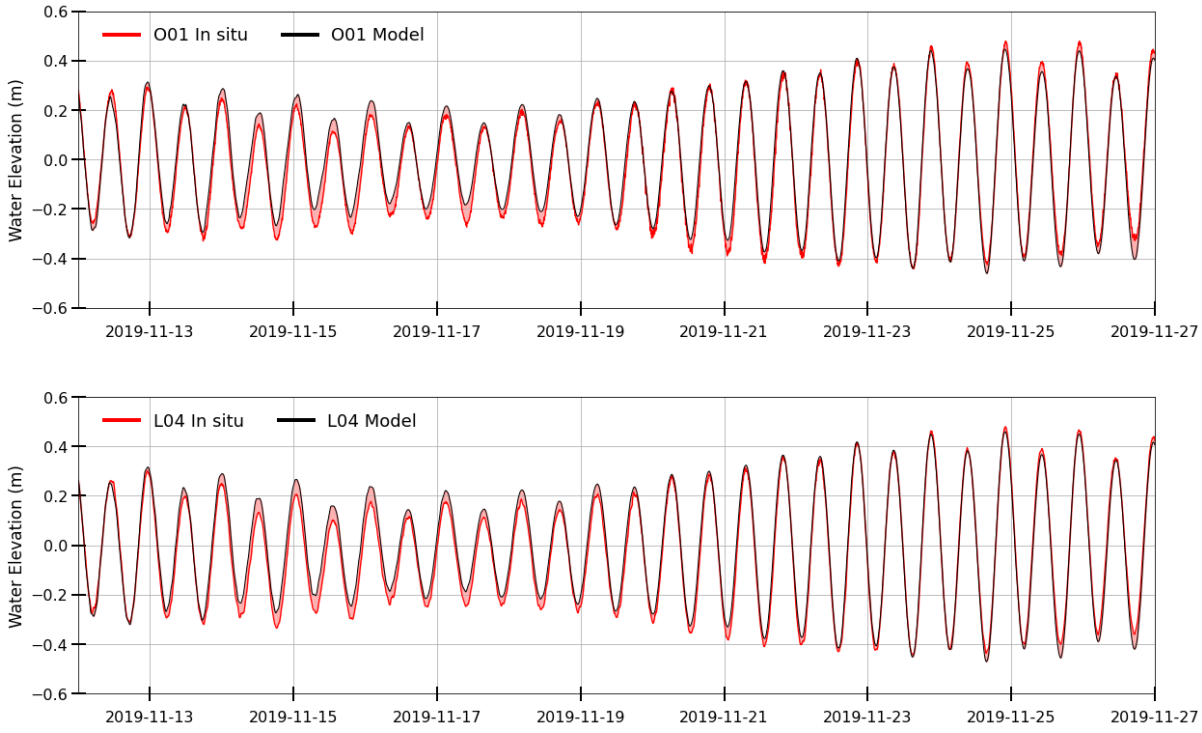

Figure 7: During Leg 2, comparison between *in situ* and modeled tides for one oceanic station (O01) and one lagoon station (L04).

Figure 8 compares model and *in situ* data for the three ADCP sensors bordering the Rikitea lagoon. Model outputs are generally in good agreement with the observations (Table 2), although modeled depth-averaged current speeds are generally underestimated for all sensors, and depth-averaged current directions do not match exactly the main sensors directions (Figure 8). The u-component for Aquadopp-1 sensor is poorly reproduced (R^2=0.06) and this is likely explained by a local topography effect, the sensor being deployed on a steep slope just in front of the Mangareva – Aukena sill, a configuration that the model does not

reproduce well. Also, Aquadopp-1 remains mostly controlled by tide in the model, with two main directions, while *in situ* data shows a dominance of ~180° southward direction.

Table 2: Coefficient of determination R^2 of the linear regression and root-mean-square error RMSE (in $m.s^{-1}$) achieved when compared modeled current speed components with in situ *values for the three* in situ *sensors moored around the Rikitea sub-lagoon.*

	S50-2		Aquadopp-1		Aquadopp-2	
Model variable	**R^2**	**RMSE**	**R^2**	**RMSE**	**R^2**	**RMSE**
U speed component	0.49	0.08	0.06	0.08	0.65	0.10
V speed component	0.59	0.13	0.70	0.03	0.44	0.05

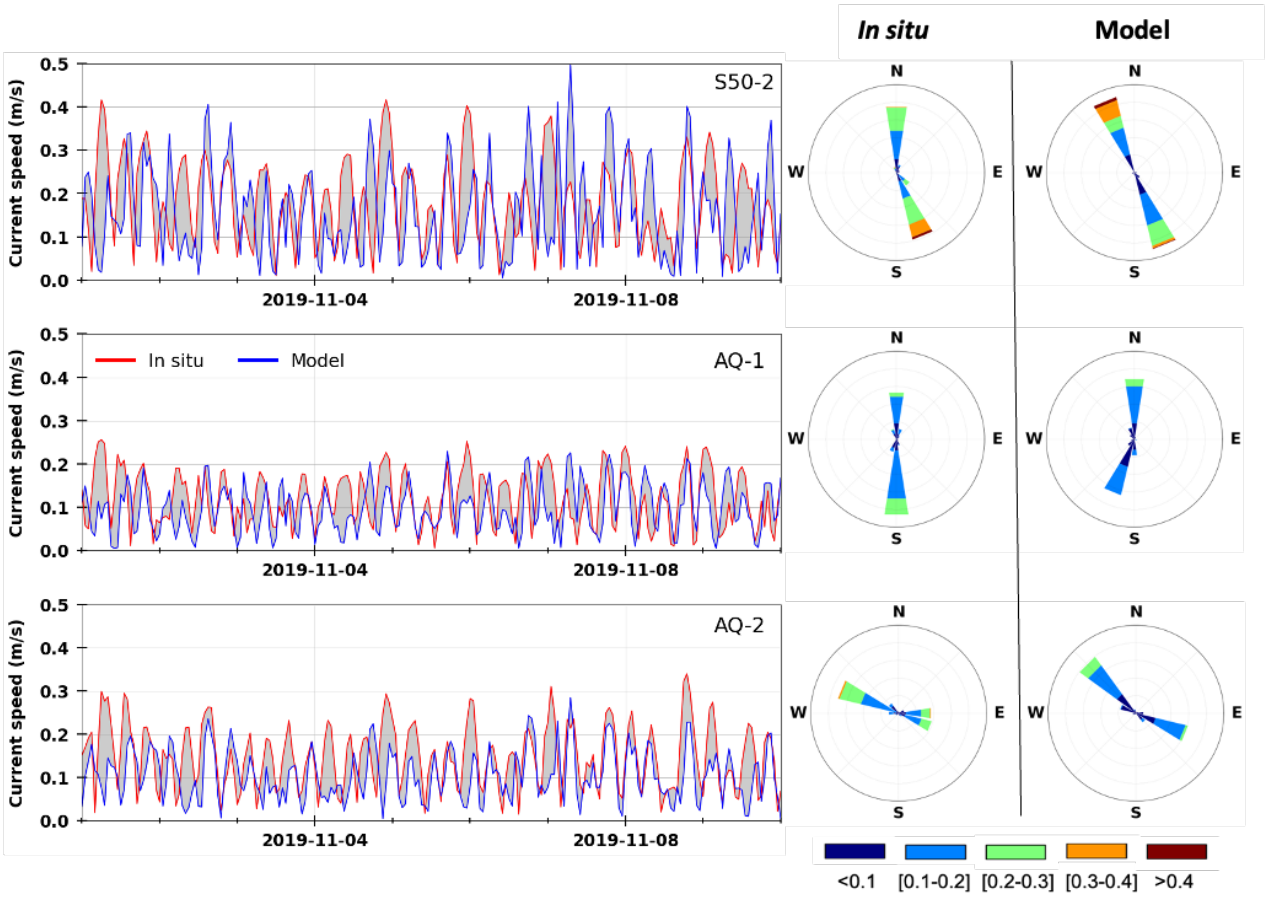

Figure 8: For Leg 2, comparison of *in situ* and modeled depth-averaged current speeds (time series) and directions (wind roses) (see color legend at the bottom in m/s) for the three S50-2, AQ-1 and AQ-2 sensors around the Rikitea sub-lagoon. The differences between measured and modelled current speeds are highlighted in grey. By convention, current direction is the angle from which the current is coming from (0°=North).

3.4 Larval dispersal modelling

The results of the four scenarios of larval dispersal are summarized in Figure 8ç which presents the percent of larvae emitted by each station that remains in the spat collection area since the virtual spawning. The percentages shown in Figure 8 are taken every day at midnight. The scenarios all appear very contrasted and the percentage of larvae remaining in the designated spat collection area is strongly related to the wind condition used for the simulation.

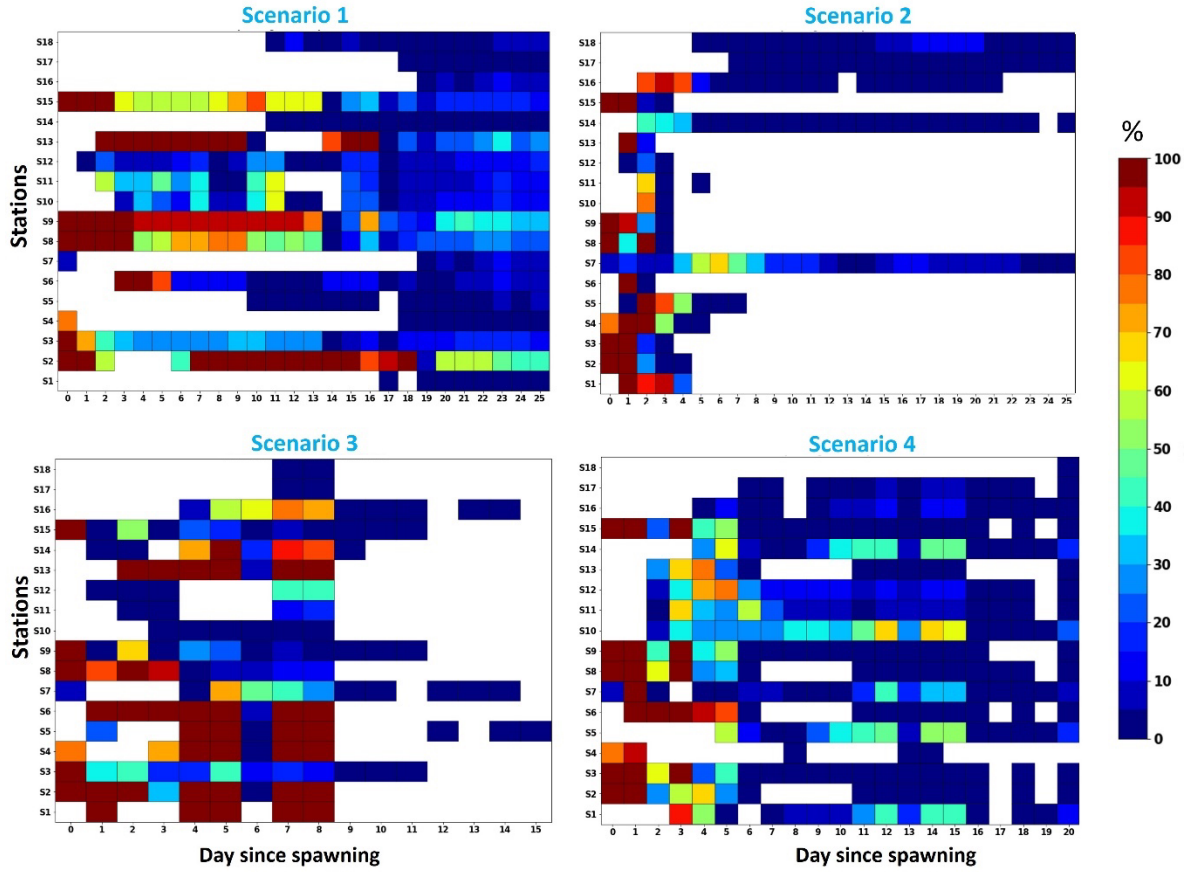

Figure 9: Results of the four dispersal scenarios, with the percentage (color bar) of emitted larvae and still present in the designated spat collecting area for each simulation day (x-axis) and for each of the 18 stations (y-axis) (Figure 2). The white color indicates the absence of larvae (0%).

The scenarios are contrasted: the “no wind” Scenario 1 shows high percentages of retention after 25 days for every release stations, even if at some moment for some stations the percentage is nil (before Day 18), but it increases again, suggesting a back and forth movement around the spat collection area. Conversely, the constant “NE wind” scenario 2

suggests that few sites can contribute, even minimally, to a potential collection in the PLD > 10 days period, with a very quick flush of the larvae outside the spat collection area. The two realistic simulations (Scenarios 3 and 4) confirm these two trends, namely retention during low wind, but quick exports of virtually all larvae outside the spat collection area as soon as the wind blows. For instance, simulation 3 shows a sharp decrease in retention in the spat collection area as soon as a strong SE wind is established on Day 9 of the simulation. Figure 10 displays the movement of larvae in the lagoon from the 18 sources for the first 12 days of this scenario. The impact of the E-SE wind is dramatic: at Day 8 and 9, and especially when the SE wind kicks off, virtually all larvae are pushed towards Mangareva Island, and leave the spat collection zone almost totally free of larvae. Days 10 and 11 with SE winds maintain this situation. Return of the larvae did not occur afterwards in this simulation. The simulation 4 in Figure 9 has a different dynamic with more frequent north wind, even if overlapping the previous scenario temporally. In this case, several wind shifts maintain some larvae (excepted for S4 station) in the collection area even after 20 days (< 20%). We note that larvae from several stations (S2, S4, S6, S8, S13) reach a nil level before larvae are brought back again to the spat collecting area. The stations in the far north (S18) or east of Mangareva (S17) can contribute, but this is strongly dependent on the wind sequence (see S17 contrasting scores between scenarios 3 and 4, Figure 9).

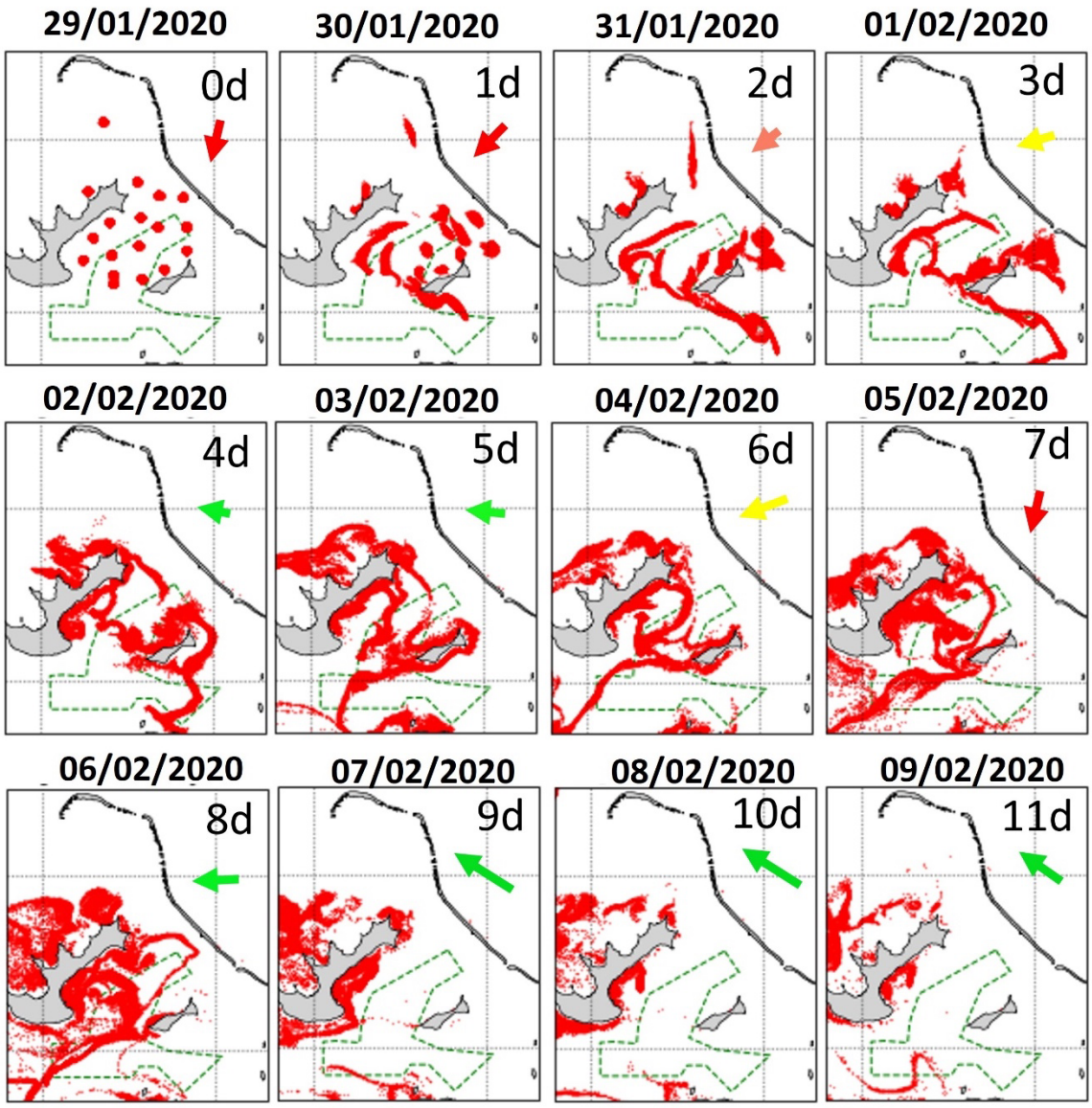

Figure 10: Larval dispersal for Scenario 3 during realistic wind conditions. The spat collection zone is shown with a green contour line. The 18 spawning stations are shown (as in Figure 2), with their initial larval distribution at day 0 (0d). Larvae broadcasted from all stations are shown in the same color here, as the general behavior of dispersal is of interested first. The plots must be understood as: for a day D the map shows the initial conditions, then 24h of realistic wind (average speed and direction on day D symbolized by the arrow, see color legend in Figure 6) blows over the lagoon. The subsequent map at day D+1 is the result of the action of this day D wind, and then the wind at D+1 is applied. The first 12 days of simulations are shown.

4. Discussion

This study presents for the first time in a pearl farming context the full suite of steps to perform in the most rigorous possible way an applied exercise based on numerical modelling and *in situ* physical oceanography observations. Previously, we already detailed some connectivity applications using model sensitivity analyses (Thomas et al., 2012b, 2014, 2016; Andréfouët et al., 2021), but without presenting the necessary backbone of model calibration/validation steps that were performed elsewhere. Fijian sites were also studied with numerical models but without any *in situ* physics measurements (Lal et al., 2016). For restocking applications in particular, the most recent Violette et al. (2023) study only presented and used the end results of the connectivity scenarios for three atolls, but not the model or its calibration with *in situ* data. For Takaroa atoll, André et al. (2022a) gave more details but no *in situ* currents, tide, or weather data. Here, for a complex site, the reader is provided with the full suite of *in situ* sampling results, the oceanographic context, model development and trials, and connectivity-based restocking application. In a sense, this shows the maturity of the development of these type of tools and their level of integration, but it is also reminder of the different complex steps required to make a well constraint exercise, including months of field surveys, deployment of an adequate array of sensors, bathymetry modelling, 3D circulation model tuning and validation, and running a variety of simulations; The last two steps require super-computing capacities to run simulations in an acceptable time frame (3 days per scenario).

For coral reef and lagoon environments, beyond pearl farming, connectivity-based applications have rarely used a time series of *in situ* physics data, if any. Storlazzi et al. (2017) for instance used satellite GPS-tracked ocean surface current drifters to compare observed and modeled current speeds at the time of coral spawning events in a marine protected area context. Conversely, there is a growing coral reef/lagoon physics literature but that may not immediately develop connectivity and management applications afterwards (e.g., Tamura et al., 2007; Rogers et al., 2016; Grimaldi et al., 2022). Generally, in coral reef and lagoon connectivity studies, the emphasis is on the biological data, without much information on the actual physical processes at stake and their accurate representation. This is however a strong mistake, as correct representation of the circulation is required for accurate dispersal modelling, especially at small spatial and temporal scales within the lagoons and adjacent to

coral reefs. Future work, in Gambier or elsewhere, will detail the sensibility of connectivity outputs to physical forcing representation, and how quickly connectivity results can be inaccurate without a proper physical characterization or model set-up.

For the farmers and managers, the important information lies in Figure 9. From the variety of situations shown in Figure 9, it is apparent that the type of short-term wind conditions occurring after a spawning event, or throughout the spawning period if it is extended, will be critical for the maintenance of larvae around the spat collection area, and therefore will likely influence spat collection rates as well. From our simulations, strong to moderate sustained east to southeast winds are unlikely to lead to good collecting rates. These are generally more dominant in the winter than in the collecting season, but a single episode in the summer can have large consequences if it is significant or it occurs at a time when larvae are ready to settle. To refine our simulations, it is necessary to have a good understanding of what can be the spawning frequency, and/or the triggers of spawning. Some information for Gambier is available in Le Moullac et al. (2012) but no "rules" or quantitative mechanisms that may trigger spawning are provided. Lo-Yat et al. (2022) also discuss the fact that generalization between different island and atolls is not granted when trying to define environmental predictors of larval abundance or spat collection rates. Local knowledge is needed. More actualized data are needed also. Indeed, the last confirmed three years of disastrous spat collecting (2020, 2021, and 2022) occurred in La Niña years. The 2023 year seems to follow the same path (DRM, pers. com.). A long-term monitoring of oyster reproduction should therefore require the inclusion of El Niño, La Niña and normal years. Conversely, farmers in Gambier reported they had exceptional spat collection rates in the warm 2016-2017 season (Liao, 2019), in the tail of a strong El Niño year (Edmunds, 2017). As in 2023, part of the stock used for pearl grafting still comes from this remarkable 2016-2017 collecting year.

The ERA5 wind data can be used to detect unusually calm years with simple exploratory statistics (Figure 11). A 20 days low wind duration period is interesting as it roughly corresponds to the expected pelagic larval duration of *Pinctada margaritifera* in Gambier (Sangare et al., 2020), hence we search for periods during which approximately 20 days of low wind occurred. For instance, January 2017, January 2012, and March 2013 are the only months in 20 years that have 20 days below the 4 $m.s^{-1}$ wind speed threshold. These 3 months

stand out as potentially favorable years for spat collecting, should spawning occur at these times. January 2017 is also the month with the highest numbers of days below 2 $m.s^{-1}$ (6 days). These anomalies could explain well the 2017 collecting scores, in agreement with our modelling findings showing that low wind is required to maintain larvae in the Rikitea lagoon. It is however likely that other variables (sea surface temperature, chlorophyll as a proxy of food abundance, etc.) that can also co-vary with temperature are worthy of investigation as well to help explaining spat collecting rates (Figure 11).

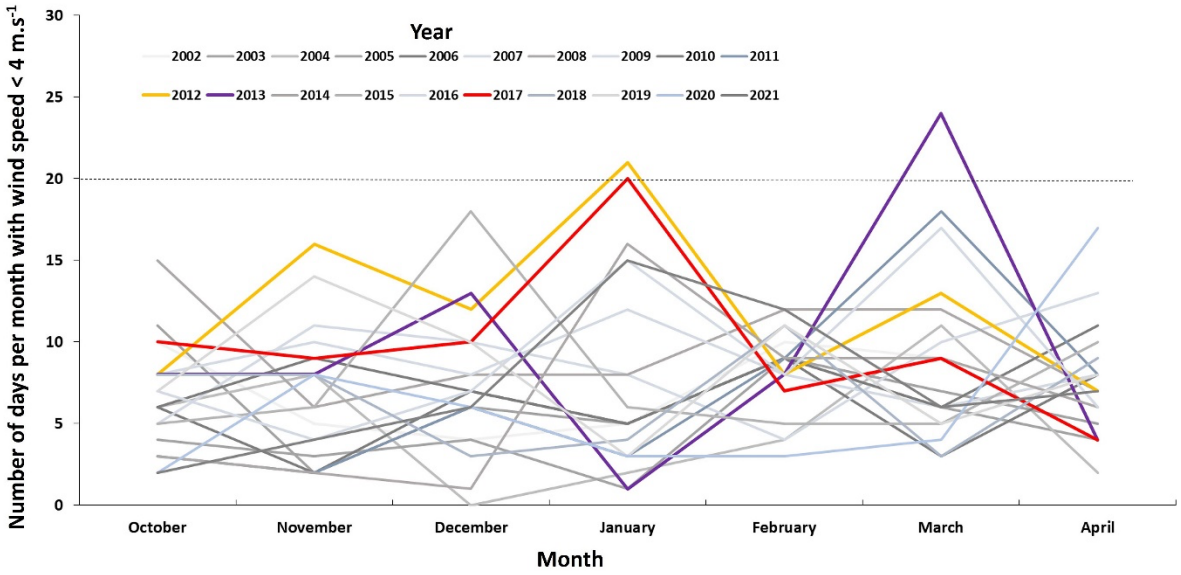

Figure 11: Number of days below the 4 $m.s^{-1}$ wind speed threshold for each month of the year between 2002 and 2022. The colored years are those for which at least one month of the warm season (October-April) reaches this threshold for at least 20 days.

While it would be possible to run additional scenarios and compare the inter-annual wind variability with additional statistics to try to explain spat collecting, to make the exercise complete and conclusive we simply miss historical inter-annual spat collecting data. Here, we could validate the hydrodynamic model with *in situ* physical oceanography data against a high resolution model (100 m), and we achieve results at a spatial resolution within the guidelines for coastal modelling work recently put forward by Ward et al. (2023), yet, they do not provide validation data for the biological component of this story. These can be provided only by the farmers. Unfortunately, these data are not available, and simply does not exist. This is again a call here for participatory research with the involvement of pearl farmers if they could collect and make available some spat collecting statistics results. This will be useful for everyone: researchers, managers and farmers. Farmers, in Gambier and elsewhere, are

increasingly grouped into collective committee that altogether discuss their current common issues. Information sharing, while not necessarily popular between farmers, should however be considered and discussed in these committee for the benefits of all. Other possibilities to validate the simulations and scenarios presented here, or others coming in the future, can be based on experimental spat collectors (as in Liao, 2019 or Lo-Yat et al., 2022) but that can be only limited compared to the coverage provided by farmers, *in situ* oyster larval census (as in Thomas et al., 2012a) although this poses significant logistical and larvae identification problems, and genetics with parental or population analysis as in Reisser et al. (2020) and Andréfouët et al. (2021).

The various connectivity and larval dispersal scenarios presented here are important inputs for management actions in the pearl farming context. In particular restocking of pearl oyster benthic populations is seen as an important action to help maintaining spat collection in the long run (Violette et al., 2023), and pearl farming. The four dispersal scenarios presented here are already useful to identify restocking sites despite the apparent strong variability between scenarios. The scenario 4, the most realistic, suggests that stations S1, S5, S7, S10 and S14 would be the most interesting for restocking in order to enhance the reproduction and dispersal potentials. Series of scenario could be run to multiply the situations, which could be afterwards synthetized meaningfully with multivariate analysis and with logistical criteria (distance to farms, depth range) as in Violette et al. (2023). Overall, the most likely area for restocking to be recommended is in the central and northern parts of the Rikitea lagoon within a polygon defined by S14-S16-S7-S2-S10 (Figure 3). Clearly, from Figure 9, more precise identification of restocking sites for a given year will depend on the wind conditions after spawning, an information that remains however totally impossible to forecast weeks in advance in the current state of knowledge.

The suite of operations and tools we have implemented for this study are complex and costly. In one hand, it is difficult to just call for the replication of these approaches to all farming sites. It is not realistic to develop the same approach for 20 sites. Yet, on the other hand, since the first feasibility workshop conducted on these approaches in 2004 (Andréfouët et al., 2006), now four different pearl farming sites have a 3D hydrodynamical model running (Ahe, Takaroa, Raroia and thus Gambier), in contrasted lagoons. More sites have been

instrumented to collect physical oceanography data (including Takapoto and Apataki) or have been the object of oyster stock assessment (Bionaz et al., 2022). All combined, they provide a suite of capable tools and critical knowledge to understand better the processes relevant for pearl farming in a variety of lagoons, submitted to a variety of environmental and oyster stock conditions. Specifically for Gambier, future work is needed to better study the entire lagoon, and not just the Rikitea sub-lagoon. Here, we have not detailed all the *in situ* data and their comparisons with modelled data (namely, for the ADCP S20-1, S20-2, and S50-1 sensors), but results are in the range of what is shown here for the sensors around the Rikitea lagoon (Figure 8). The 3D model can now be used to understand the circulation in the entire lagoon. All measurements will be this time at play. Ideally, *in situ* ADCP measurements during Leg 1 would have been useful to assess the circulation when it is forced by high oceanic waves, that were absent from the Leg 2. Future field work may consider mooring ADCP during the winter as well to better refine the model in all possible conditions. We expect that more dispersal scenarios will be also investigated to inform restocking programs, and in general all activities requiring locally optimized spatial planning decisions.

Acknowledgements

This study was funded by a grant 8345/VP/DRM from DRM to IRD and by the grant ANR-16-CE32-0004 MANA (Management of Atolls project) from Agence Nationale de la Recherche. Instruments were provided by the Direction des Ressources Marines, OTI project, Contrat de Projet France-French Polynesia, Program 123, Action 2, 2015–2020. We thank our colleagues Bertrand Bourgeois, John Butcher, and David Varillon for their help in the field, as well as Emile Puputauki for his boat captain skills. Sébastien Petton helped for the MARS3D model set-up. Multibeam lagoon bathymetry data were funded by DRM through a grant with the Geopolynesie Company. The authors also acknowledge the *Pôle de Calcul et de Données Marines* (PCDM) for providing DATARMOR storage and computational resources (http://www.ifremer.fr/pcdm). We acknowledge the reviewers for their useful suggestions.

References

Amrari, S., Bourassin, E., Andréfouët, S., Soulard, B., Lemonnier, H., Le Gendre, R., 2021. Shallow water bathymetry retrieval using a band-optimization iterative approach: application to New Caledonia coral reef lagoons using Sentinel-2 Data. Remote Sensing 13, 4108. https://doi.org/10.3390/rs13204108

André, L.V., Chinain, M., Gatti, C.M., Liao, V., Van Wynsberge, S., Tedesco, P., Andréfouët, S., 2022a. A systematic prioritization approach for identifying suitable pearl oyster restocking zones following a mass mortality event in Takaroa Atoll, French Polynesia. Marine Pollution Bulletin 176, 113472. https://doi.org/10.1016/j.marpolbul.2022.113472

André, L.V., Van Wynsberge, S., Chinain, M., Gatti, C.M.I., Liao, V., Andréfouët, S., 2022b. Spatial Solutions and Their Impacts When Reshuffling Coastal Management Priorities in Small Islands with Limited Diversification Opportunities. Sustainability 14, 3871. https://doi.org/10.3390/su14073871

Andréfouët, S., Ouillon, S., Brinkman, R., Falter, J., Douillet, P., Wolk, F., Smith, R., Garen, P., Martinez, E., Laurent, V., Lo, C., Remoissenet, G., Scourzic, B., Gilbert, A., Deleersnijder, E., Steinberg, C., Choukroun, S., Buestel, D., 2006. Review of solutions for 3D hydrodynamic modeling applied to aquaculture in South Pacific atoll lagoons. Marine Pollution Bulletin 52, 1138–1155. https://doi.org/10.1016/j.marpolbul.2006.07.014

Andréfouët, S., Chagnaud, N., Chauvin, C., Kranenburg, C., 2008. Atlas of the French Overseas Coral Reefs, Centre IRD de Nouméa, Nouméa, Nouvelle-Calédonie. CD-ROM.

Andréfouët, S., Charpy, L., Lo-Yat, A., Lo, C., 2012. Recent research for pearl oyster aquaculture management in French Polynesia. Marine Pollution Bulletin 65, 407–414. https://doi.org/10.1016/j.marpolbul.2012.06.021

Andréfouët, S., Le Gendre, R., Thomas, Y., Lo-Yat, A., Reisser, C.M.O., 2021. Understanding connectivity of pearl oyster populations within Tuamotu atoll semi-closed lagoons: Cumulative insight from genetics and biophysical modelling approaches. Marine Pollution Bulletin 167, 112324. https://doi.org/10.1016/j.marpolbul.2021.112324

Andréfouët, S., Lo-Yat, A., Lefebvre, S., Bionaz, O., Liao, V., 2022. The MANA (MANagement of Atolls, 2017–2022) project for pearl oyster aquaculture management in the Central Pacific Ocean using modelling approaches: Overview of first results. Marine Pollution Bulletin 178, 113649. https://doi.org/10.1016/j.marpolbul.2022.113649

Aucan, J., Vendé-Leclerc, M., Dumas, P., Bricquir, M., 2017. Wave forcing and morphological changes of New Caledonia lagoon islets: Insights on their possible relations. C. R. Geosci. 349, 248–259. https://doi.org/10.1016/j.crte.2017.09.003

Bionaz, O., Le Gendre, R., Liao, V., Andréfouët, S., 2022. Natural stocks of *Pinctada margaritifera* pearl oysters in Tuamotu and Gambier lagoons: New assessments, temporal evolutions, and consequences for the French Polynesia pearl farming industry. Marine Pollution Bulletin 183, 114055. https://doi.org/10.1016/j.marpolbul.2022.114055

Demerliac, A., 1974. Calcul du niveau moyen journalier de la mer. Rapport du service hydrographique de la marine 741, 49–57.

Dumas, F., Le Gendre, R., Thomas, Y., Andréfouët, S., 2012. Tidal flushing and wind driven circulation of Ahe atoll lagoon (Tuamotu Archipelago, French Polynesia) from in situ observations and numerical modelling. Marine Pollution Bulletin 65, 425–440. https://doi.org/10.1016/j.marpolbul.2012.05.041

Edmunds, P.J., 2017. Unusually high coral recruitment during the 2016 El Niño in Moorea, French Polynesia. PLoS ONE 12, e0185167. https://doi.org/10.1371/journal.pone.0185167

Fournier, J., Levesque, E., Pouvreau, S., Pennec, M.L., Moullac, G.L., 2012. Influence of plankton concentration on gametogenesis and spawning of the black lip pearl oyster Pinctada margaritifera in Ahe atoll lagoon (Tuamotu archipelago, French polynesia). Marine Pollution Bulletin 65, 463–470. https://doi.org/10.1016/j.marpolbul.2012.03.027

Grimaldi, C.M., Lowe, R.J., Benthuysen, J.A., Green, R.H., Reyns, J., Kernkamp, H., Gilmour, J., 2022. Wave and Tidally Driven Flow Dynamics Within a Coral Reef Atoll off Northwestern Australia. JGR Oceans 127. https://doi.org/10.1029/2021JC017583

Lal, M.M., Southgate, P.C., Jerry, D.R., Bosserelle, C., Zenger, K.R., 2016. A Parallel Population Genomic and Hydrodynamic Approach to Fishery Management of Highly-Dispersive Marine Invertebrates: The Case of the Fijian Black-Lip Pearl Oyster Pinctada margaritifera. PLoS ONE 11, e0161390. https://doi.org/10.1371/journal.pone.0161390

Laurent, V., Maamaatuaiahutapu, K., 2019. Atlas climatologique de la Polynésie française. Météo France, Faaa-Tahiti, 242 p.

Lazure, P., Dumas, F., 2008. An external-internal mode coupling for a 3D hydrodynamical model for applications at regional scale (MARS). Adv. Water Resour. 31, 233e250.

Lefebvre, S., Claquin, P., Orvain, F., Véron, B., Charpy, L., 2012. Spatial and temporal dynamics of size-structured photosynthetic parameters (PAM) and primary production (13C) of pico- and nano-phytoplankton in an atoll lagoon. Marine Pollution Bulletin 65, 478–489. https://doi.org/10.1016/j.marpolbul.2012.04.011

Lefebvre, S., Verpoorter, C., Rodier, M., Sangare, N., Andréfouët, S., 2022. Remote sensing provides new insights on phytoplankton biomass dynamics and black pearl oyster life-history traits in a Pacific Ocean deep atoll. Marine Pollution Bulletin 181, 113863. https://doi.org/10.1016/j.marpolbul.2022.113863

Le Moullac, G., Tiapari, J., Teissier, H., Martinez, E., Cochard, J.-C., 2012. Growth and gonad development of the tropical black-lip pearl oyster, *Pinctada margaritifera* (L.), in the Gambier archipelago (French Polynesia). Aquacult Int 20, 305–315. https://doi.org/10.1007/s10499-011-9460-x

Liao, V., 2019. Suivi du collectage naturel. Rapport Saison 2018-2019. Gambier. DRM, Papeete, 11 p.

Lo-Yat, A., Monaco, C.J., Thomas, Y., Czorlich, Y., Le Borgne, F., Muylaert, M., Le Moullac, G., Vanaa, V., Beliaeff, B., Garen, P., 2022. Mismatch between the ecological processes driving early life-stage dynamics of bivalves at two contrasting French Polynesian lagoons. Marine Pollution Bulletin 183, 114099. https://doi.org/10.1016/j.marpolbul.2022.114099

Reisser, C.M.O., Gendre, R.L., Chupeau, C., Lo-Yat, A., Planes, S., Andréfouët, S., 2020. Population connectivity and genetic assessment of exploited and natural populations of pearl oysters within a French Polynesian atoll lagoon. Genes 11, 426. https://doi.org/10.3390/genes11040426

Rodier, M., Pinazo, C., Seceh, C., Varillon, D., 2021. Pelagic stocks and carbon and nitrogen uptake in a pearl farming atoll (Ahe, French Polynesia). Marine Pollution Bulletin 167, 112352. https://doi.org/10.1016/j.marpolbul.2021.112352

Rogers, J.S., Monismith, S.G., Koweek, D.A., Torres, W.I., Dunbar, R.B., 2016. Thermodynamics and hydrodynamics in an atoll reef system and their influence on coral cover: Atoll Thermal & Hydro-Dynamics & Coral Effects. Limnol. Oceanogr. 61, 2191–2206. https://doi.org/10.1002/lno.10365

Sangare, N., Lo-Yat, A., Moullac, G.L., Pecquerie, L., Thomas, Y., Lefebvre, S., Gendre, R.L., Beliaeff, B., Andréfouët, S., 2020. Impact of environmental variability on *Pinctada margaritifera* life-history traits: A full life cycle deb modeling approach. Ecological Modelling 423, 109006. https://doi.org/10.1016/j.ecolmodel.2020.109006

Storlazzi, C.D., van Ormondt, M., Chen, Y.-L., Elias, E.P.L., 2017. Modeling fine-scale coral larval dispersal and interisland connectivity to help designate mutually-supporting coral reef marine protected areas: Insights from Maui Nui, Hawaii. Front. Mar. Sci. 4, 381. https://doi.org/10.3389/fmars.2017.00381

Tamura, H., Nadaoka, K., Paringit, E.C., 2007. Hydrodynamic characteristics of a fringing coral reef on the east coast of Ishigaki Island, southwest Japan. Coral Reefs 26, 17–34. https://doi.org/10.1007/s00338-006-0164-z

Thomas, Y., Garen, P., Bennett, A., Le Pennec, M., Clavier, J., 2012a. Multi-scale distribution and dynamics of bivalve larvae in a deep atoll lagoon (Ahe, French Polynesia). Marine Pollution Bulletin 65, 453–462. https://doi.org/10.1016/j.marpolbul.2011.12.028

Thomas, Y., Le Gendre, R., Garen, P., Dumas, F., Andréfouët, S., 2012b. Bivalve larvae transport and connectivity within the Ahe atoll lagoon (Tuamotu Archipelago), with application to pearl oyster aquaculture management. Marine Pollution Bulletin 65, 441–452. https://doi.org/10.1016/j.marpolbul.2011.12.027

Thomas, Y., Dumas, F., Andréfouët, S., 2014. Larval dispersal modeling of pearl oyster *Pinctada margaritifera* following realistic environmental and biological forcing in Ahe Atoll lagoon. PLoS ONE 9, e95050. https://doi.org/10.1371/journal.pone.0095050

Thomas, Y., Dumas, F., Andréfouët, S., 2016. Larval connectivity of pearl oyster through biophysical modelling; evidence of food limitation and broodstock effect. Estuarine, Coastal and Shelf Science 182, 283–293. https://doi.org/10.1016/j.ecss.2016.03.010

Violette, C., Le Gendre, R., Chauveau, M., Andréfouët, S., 2023. A multivariate approach to synthetize large amount of connectivity matrices for management decisions: Application to oyster population restocking in the pearl farming context of Tuamotu Archipelago semi-closed atolls. Marine Pollution Bulletin 189, 114748. https://doi.org/10.1016/j.marpolbul.2023.114748

Visser, A. W., 1997. Using random walk models to simulate the vertical distribution of particles in a turbulent water column. Marine Ecology Progress Series, 158, 275-281.

Ward, S.L., Robins, P.E., Owen, A., Demmer, J., Jenkins, S.R., 2023. The importance of resolving nearshore currents in coastal dispersal models. Ocean Modelling 183, 102181. https://doi.org/10.1016/j.ocemod.2023.102181